Synthetic Aperture Radar

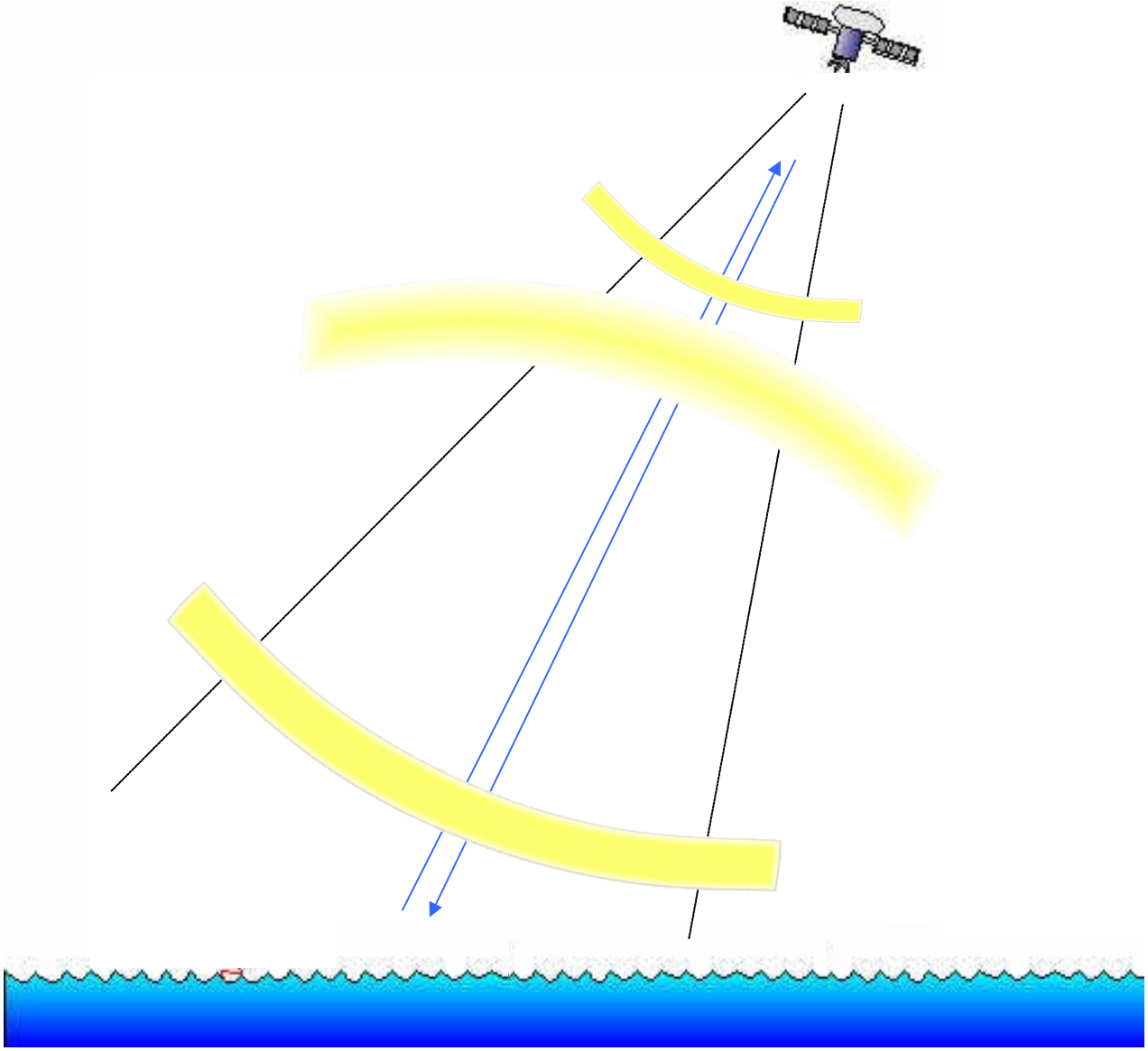

Synthetic Aperture Radar

What features can we measure?

SAR senses variation of σ_o due to modification of Bragg waves by:

- larger waves (swell)
- small-scale wind patterns
- current shear
- bottom-current/wave interaction
- slicks
- ships wakes
- sea ice
- land surface roughness
- vegetation

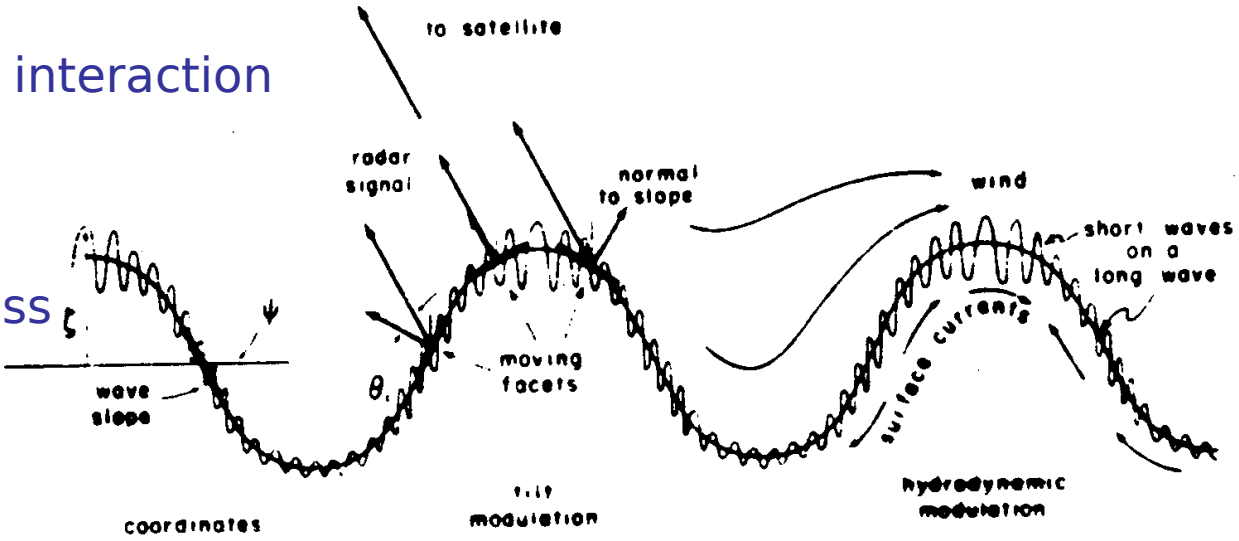

Figure 13.6 Some processes influencing SAR observations of ocean waves. Large ocean waves (a) tilt the surface, and (b) interact with short waves and distort the airflow over the surface. Both processes modulate the heights of the short waves that reflect the radar signal. And (c), large waves move the surface, thus changing the SAR image of the surface and producing wavelike patterns in the image.

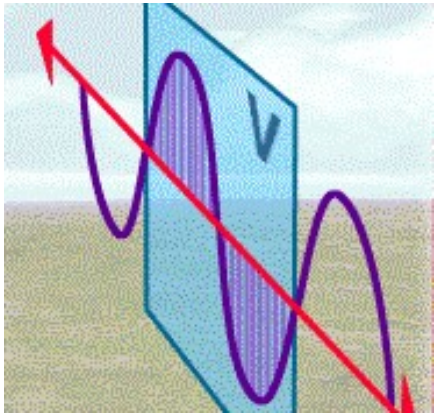

VV polarisation: studying the small-scale roughness of (capillary) waves on the water surface, VV is better than HH or cross-polarised combinations, which means it is used extensively for surface wind speed extraction.

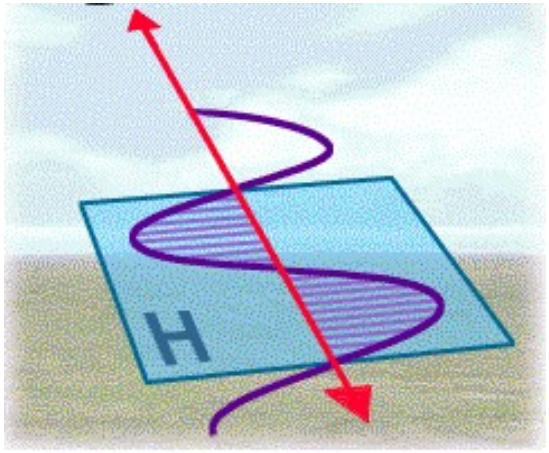

HH polarisation:the study of soil moisture, the vertically oriented crops (e.g., wheat and barley) have improved penetration with HH, allowing the backscatter to represent the soil moisture regime better rather than the crop geometry. HH is very suitable for separating marine ice and water, since it is less sensitive to water roughness than VV polarisation, thus producing an improved contrast between the two target types. For a similar reason, HH is used for ship detection.

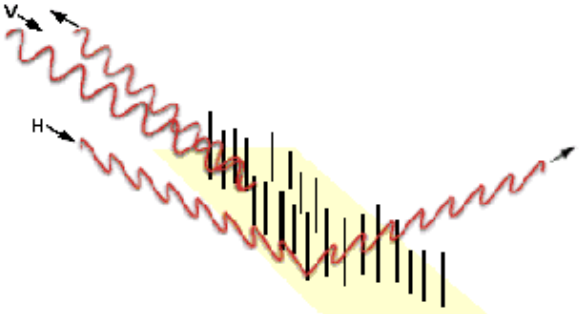

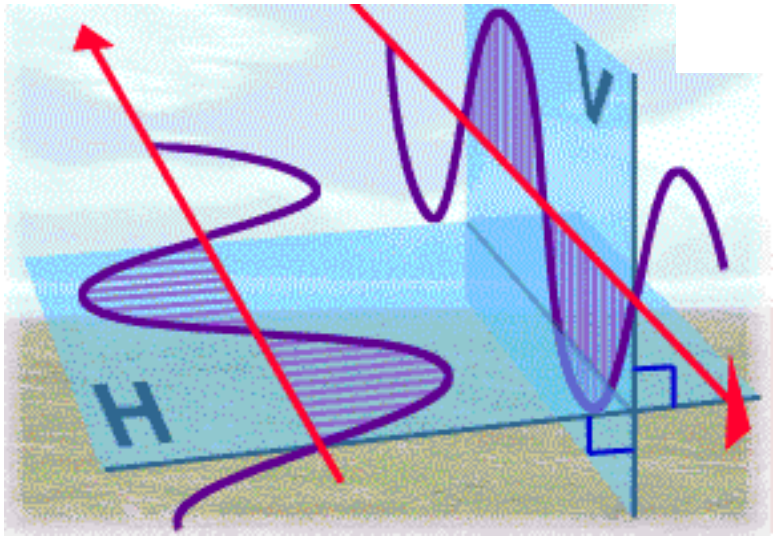

Since the backscatter from water surfaces is reduced under cross-polarised SAR illumination/detection, using the VH or HV technique is very suitable for detecting targets on the water surface, which accommodate multiple scattering necessary for depolarisation. Such targets are, for example: ship superstructures and various ice deformations (ridging,

SIR-C

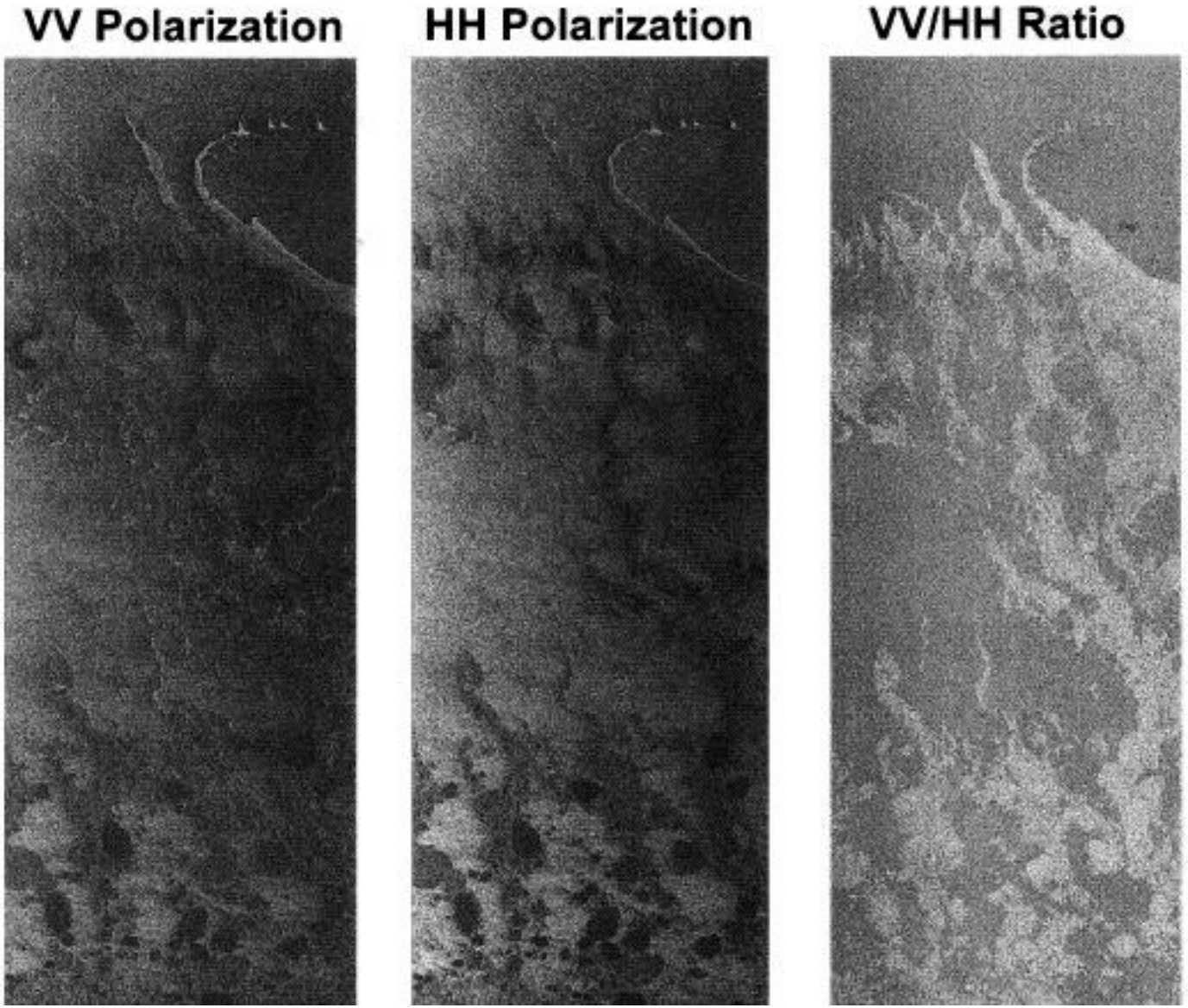

Since the ratio of VV to HH backscatter is larger than 1 for open water, but close to 1 for pack ice, the sea ice is seen to be much darker on the VV/HH ratio image, independent of incidence angle or wind conditions.

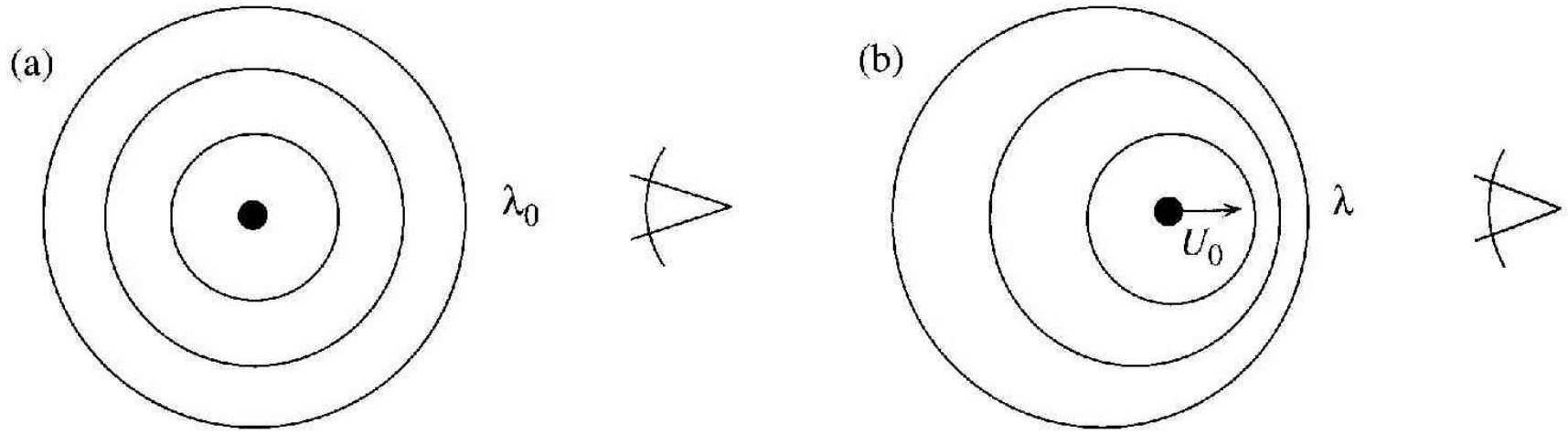

Figure 10.7. The change in wavelength associated with electromagnetic waves generated from (a) a stationary source; (b) a moving source, where the source velocity is uniform and non-relativistic.

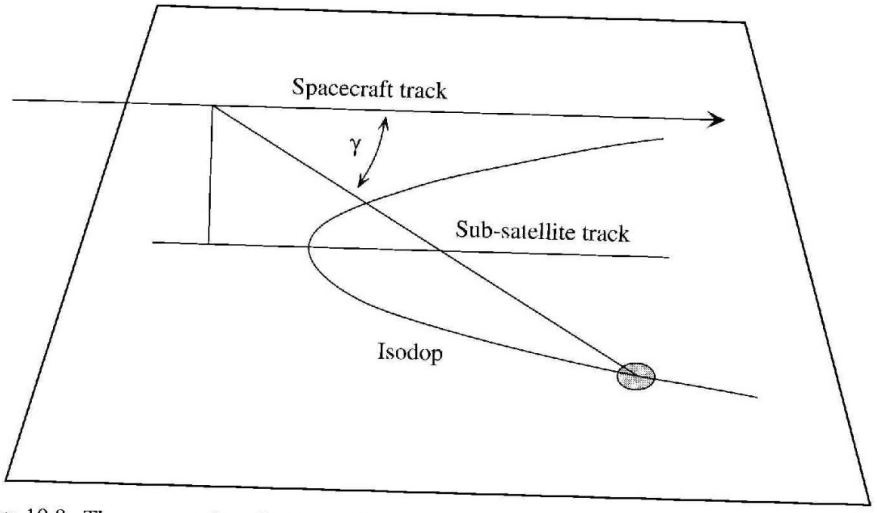

Figure 10.8. The spacecraft and sub-satellite tracks, the surface isodop, the scatterometer FOV and its view angle γ relative to the spacecraft track.

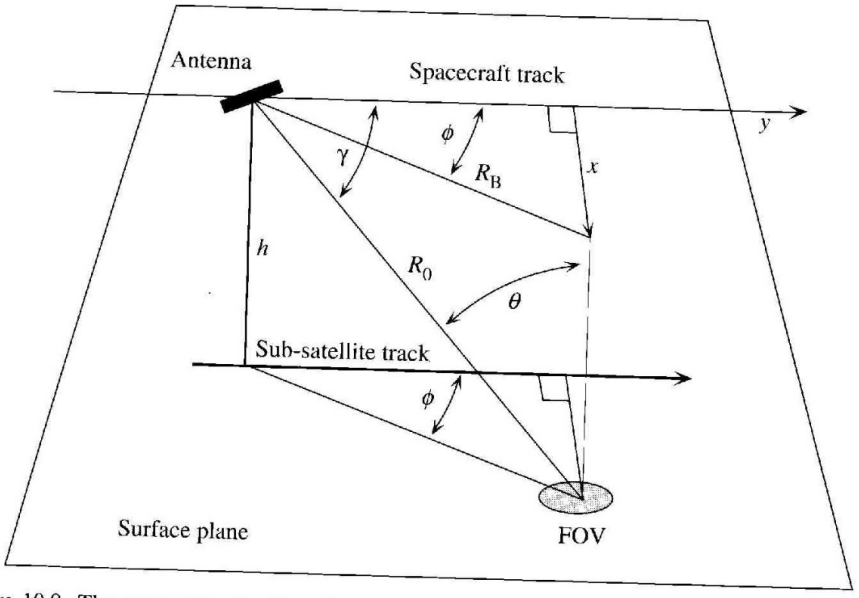

Figure 10.9. The geometry of a Doppler scatterometer above a horizontal plane, where ϕ is the azimuth angle, θ is the incidence angle and γ is the view angle relative to the spacecraft track. See text for further description.

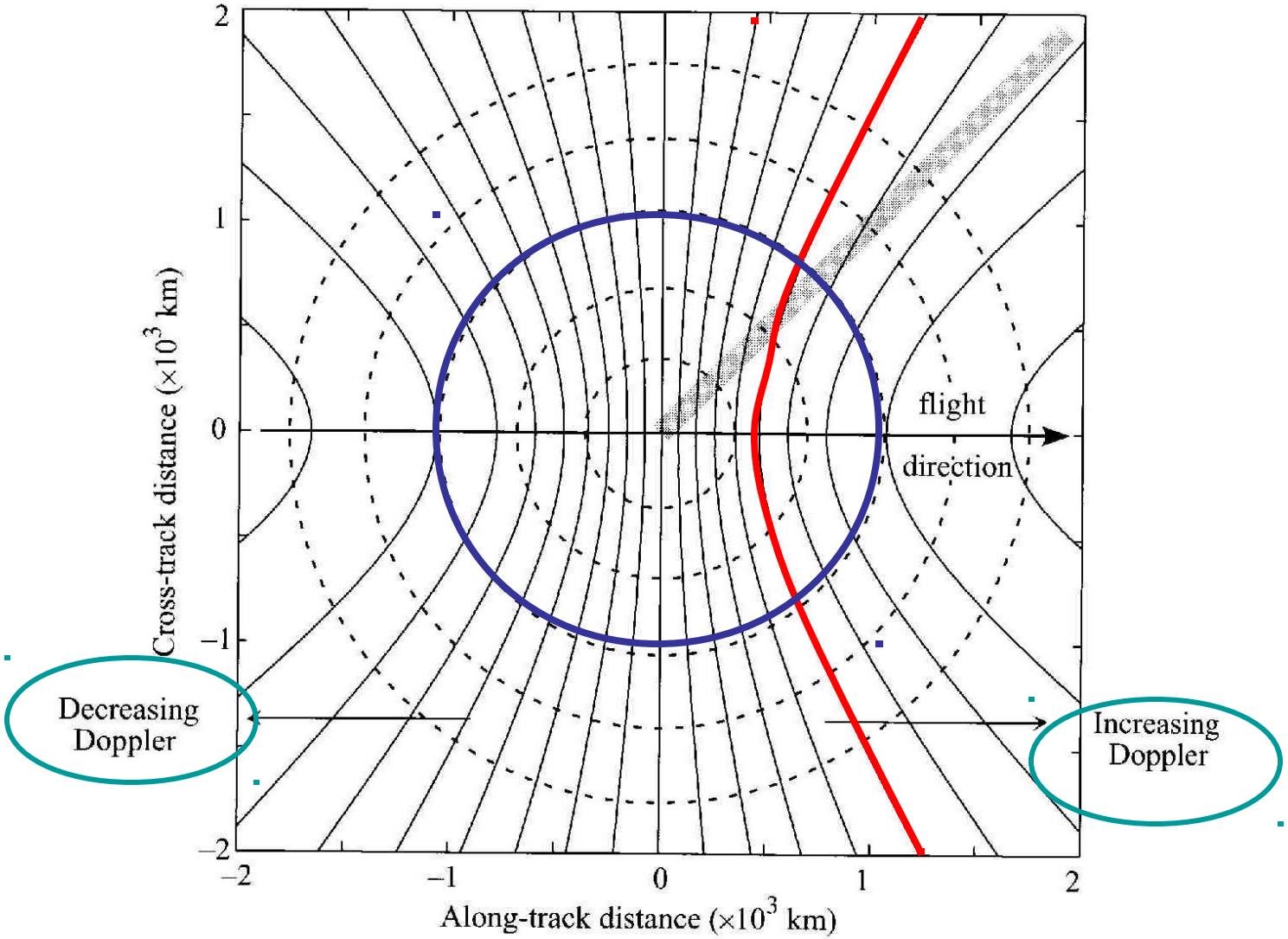

Figure 10.10. The solid lines are the isodops contoured at equal intervals of $0.1\Delta f_{max}$ on the surface plane for a satellite in horizontal motion above the plane; the dashed circles are lines of constant range (derived from Ulaby *et al.*, 1982, Equation 7.46). The origin lies directly beneath the spacecraft; the gray bar shows a typical FOV. See text for further description.

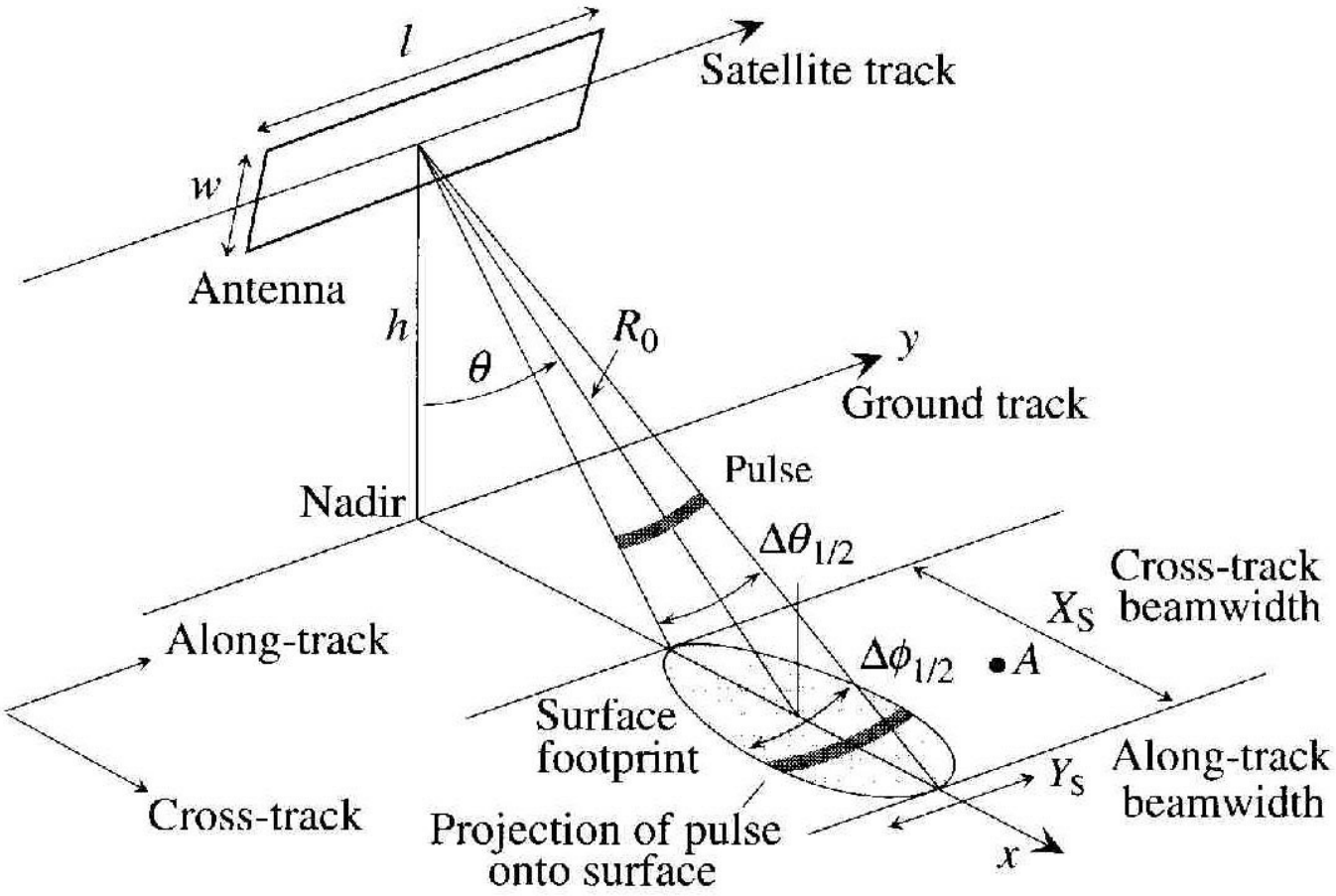

Figure 13.1. The viewing geometry for the SAR and SLR antenna: w is the antenna width; l is the length. For clarity, the along-track width of the surface footprint is greatly exaggerated relative to the cross-track; typical footprint dimensions are 3 km × 100 km. At the scale of the figure, the along-track beamwidth would be only slightly larger than the width of the line marked x.

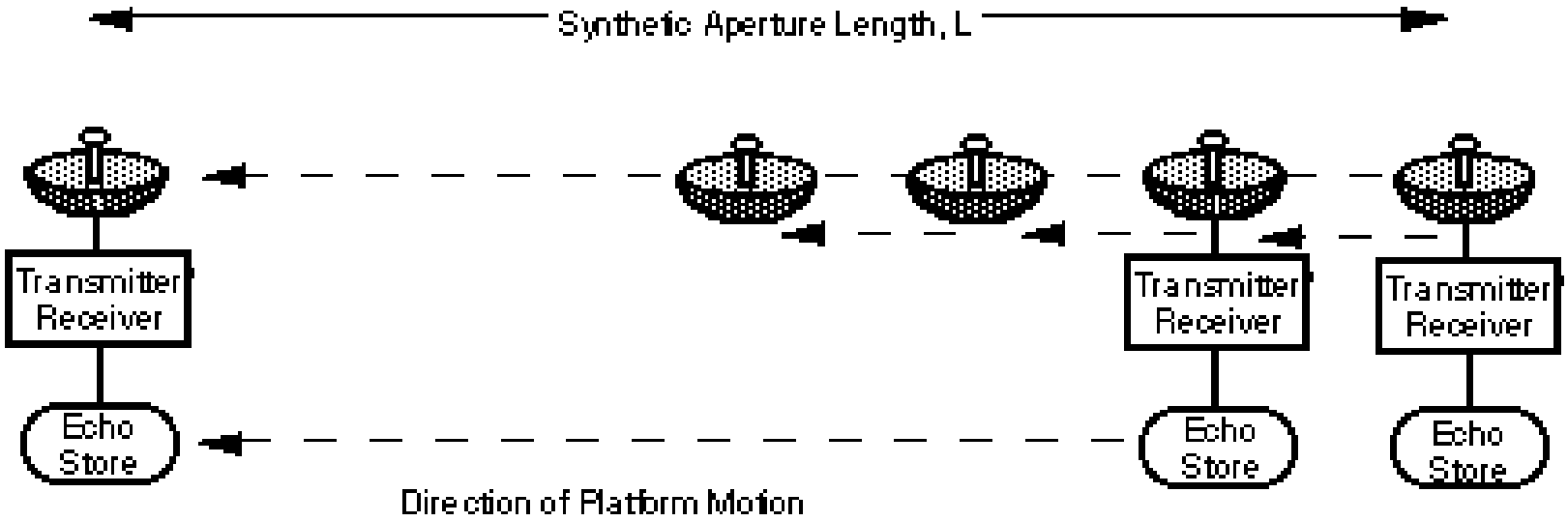
Synthetic Aperture Length, L
Transmitter Receiver
Transmitter Receiver
Transmitter Receiver
Echo Store
Echo Store
Echo Store
Direction of Platform Motion

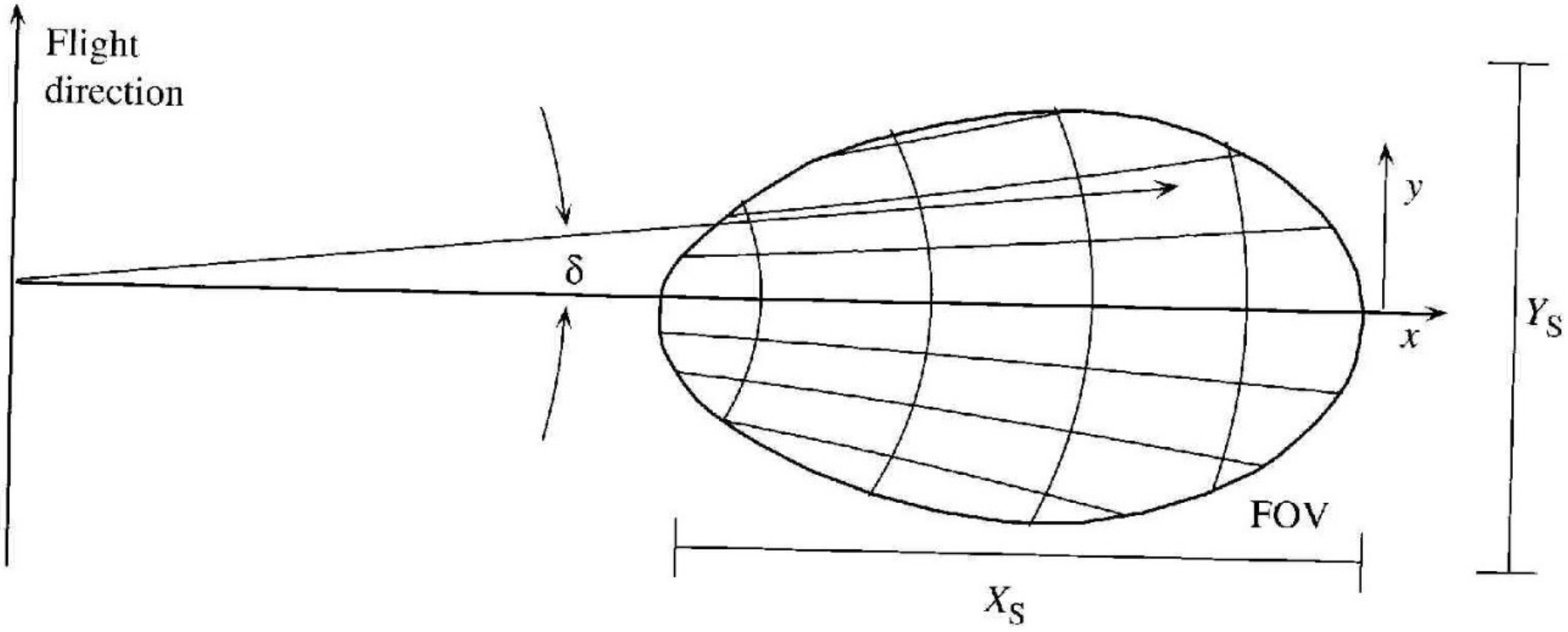

Figure 13.5. The SAR surface footprint, the lines of constant range and the orthogonal surface isodops, which lie approximately at right angles to the flight direction. The y-dimension is greatly exaggerated relative to x.

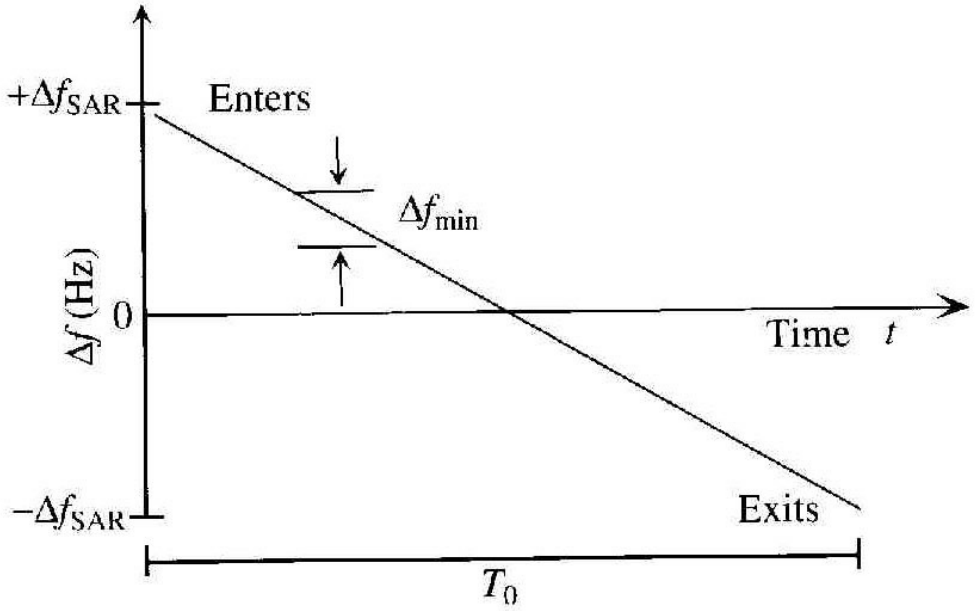

Figure 13.6. Tracking an object in frequency space across the SAR footprint, where the target enters at upper left and exits at lower right.

Synthesizing the Aperture

To get 25m resolution, we would need a very large antenna

Therefore we synthesize the aperture

$$\Delta y_{\min} = \frac{2\Delta f_{\min} \lambda_0 R_0}{2U_0}$$

for Δy_{min} = 25m

(θ=20, Δt = 5.7x10^{-8} s or 1.7GHz; $\lambda_0 = \frac{9}{\pi}$cm)

in direction along the velocity vector (dx)
use doppler shift due to spacecraft motion

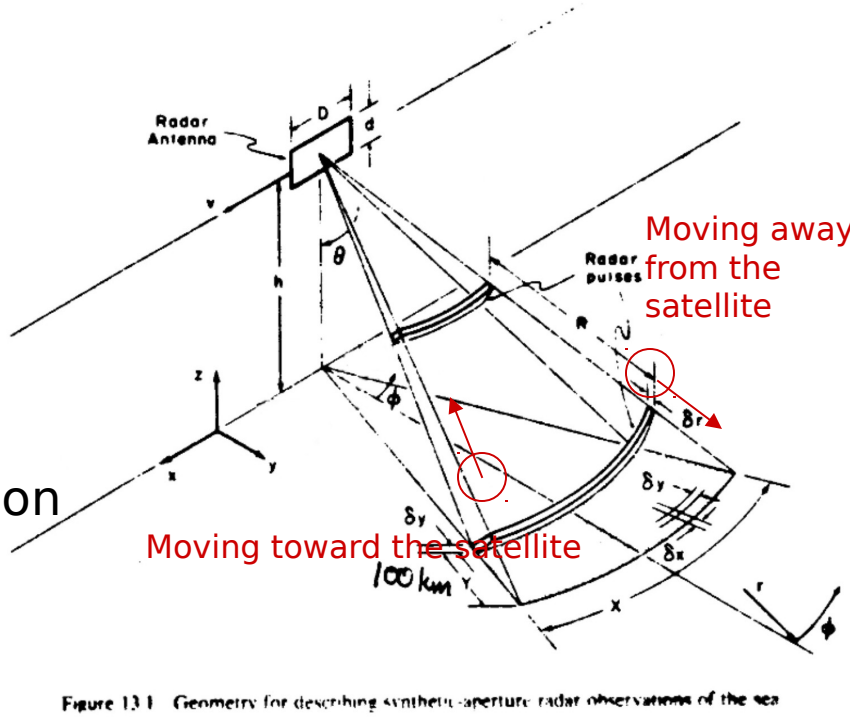

Figure 13.1 Geometry for describing synthetic-aperture radar observations of the sea

$$\Delta f_{\min} = \frac{lU_0}{\lambda_0 R_0}$$

$$\Delta y_{\min} = \frac{lU_0 \lambda_0 R_0}{\lambda_0 R_0 2U_0} = \frac{l}{2}$$

A target's backscatter will be analyzed as though it had been seen by 1000 different antennas, or correspondingly of a synthesized antenna with length equal to the distance the spacecraft passed through while it was able to get backscatter returns from that target

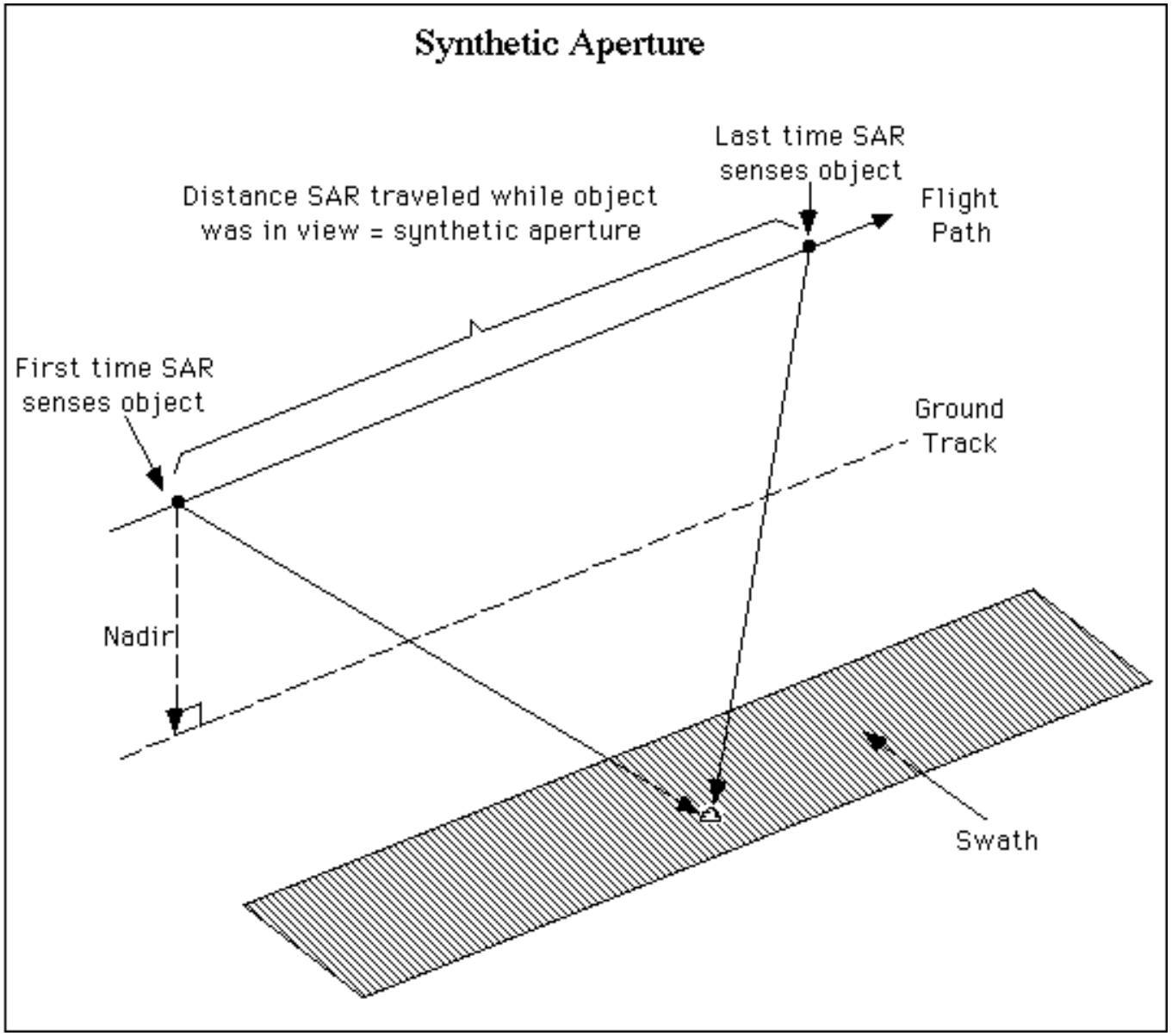

The SAR image is derived from the received power:

W(t,f)

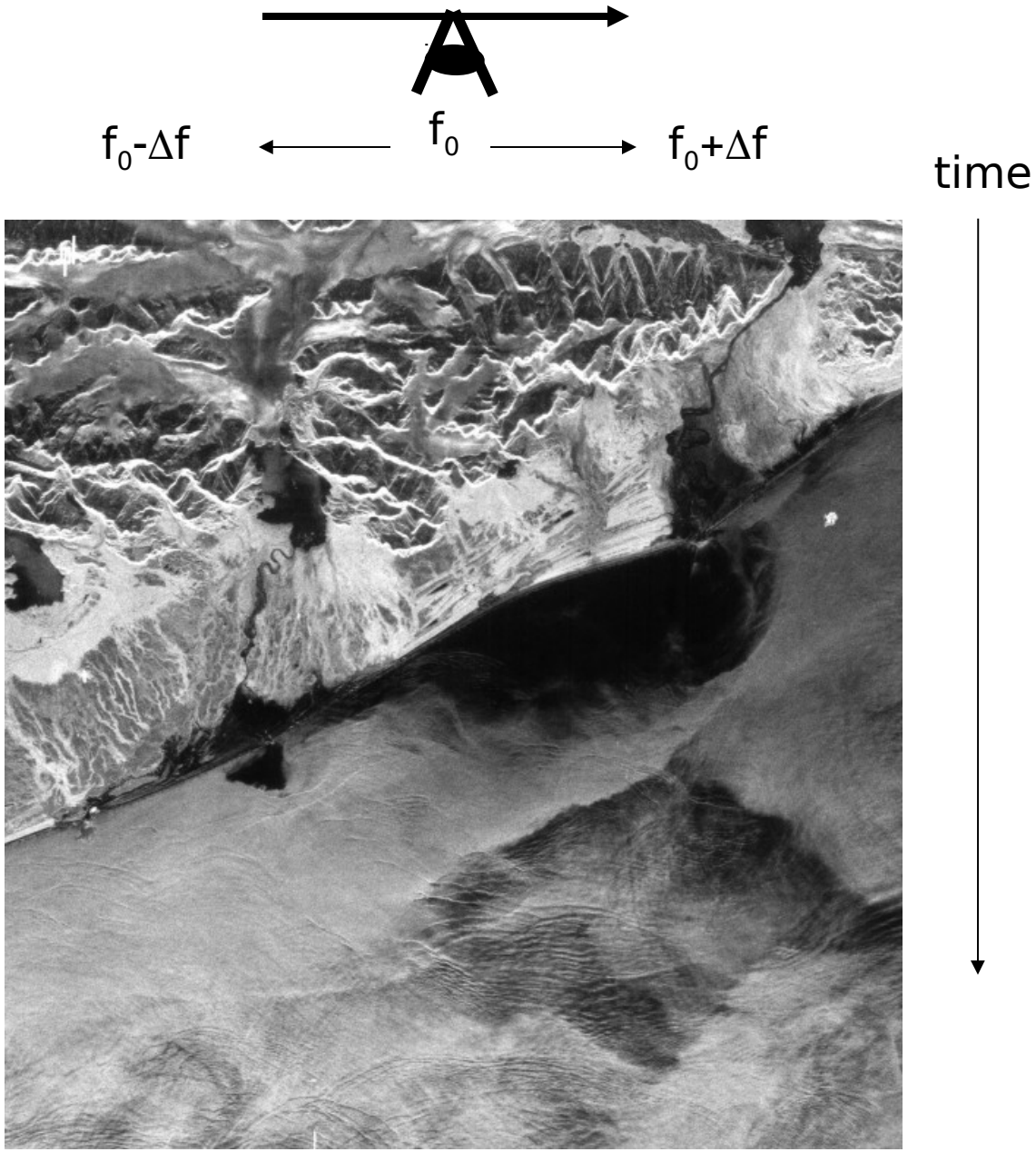

http://www.asf.alaska.edu/reference_documents/datacenters_references/sar_processing.html#prep

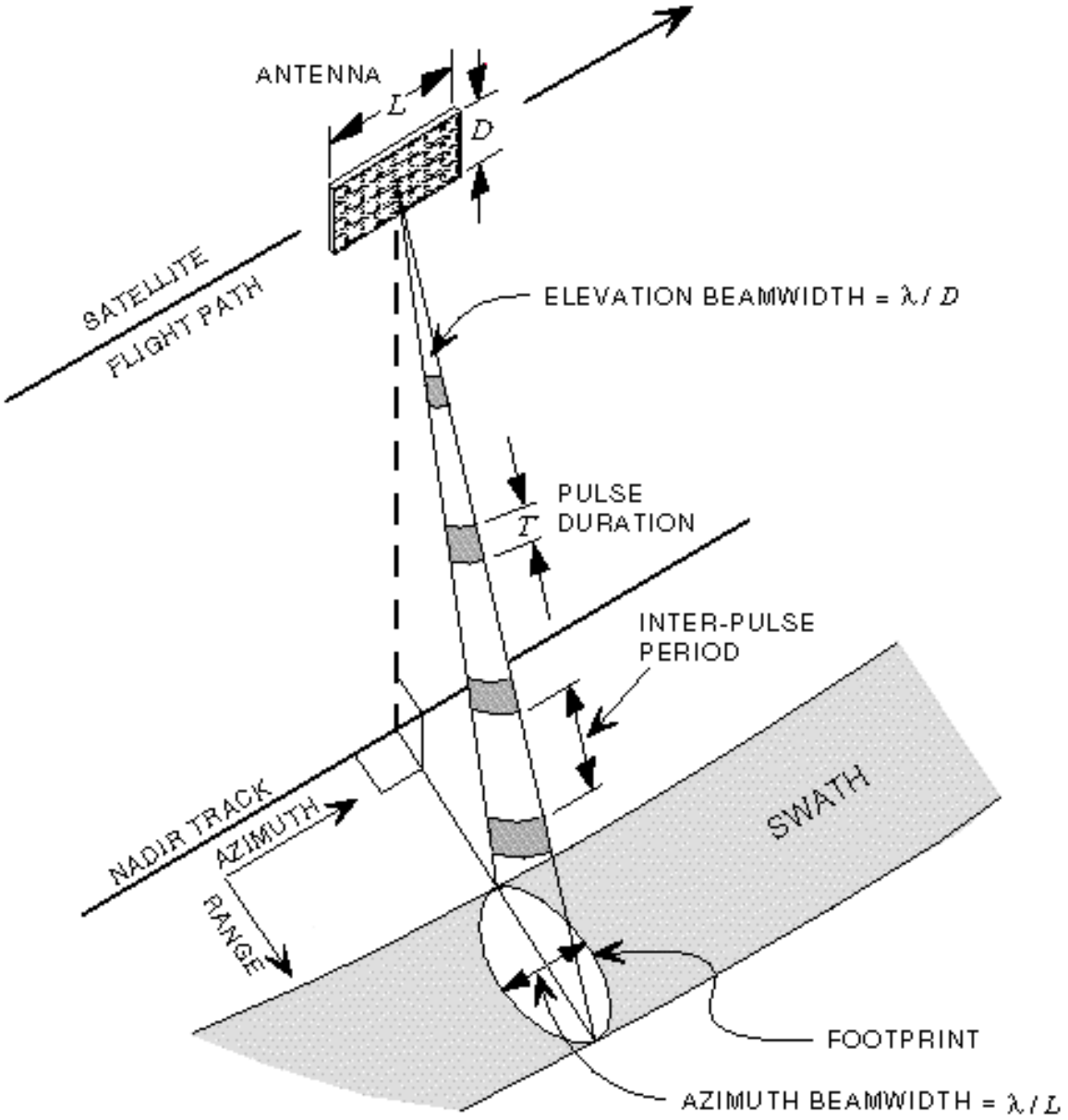
ANTENNA
L
D
SATELLITE
FLIGHT PATH
ELEVATION BEAMWIDTH = λ / D
PULSE
DURATION
τ
INTER-PULSE
PERIOD
NADIR TRACK
AZIMUTH
RANGE
SWATH
FOOTPRINT
AZIMUTH BEAMWIDTH = λ / L

Radar Bands

L-Band: 1-2 GHz, 15-30 cm wavelength (23 cm common).

S-Band: 2-4 GHz, 08-15 cm wavelength (10 cm).

C-Band: 4-8 GHz, 04-08 cm wavelength (5 cm).

X-Band: 8-12 GHz, 2.5-4 cm wavelength (3 cm).

K-Band: (u) 12-18, (a) 27-40 GHz, 1.7-2.5, .75-1.2 cm wavelength (mm).

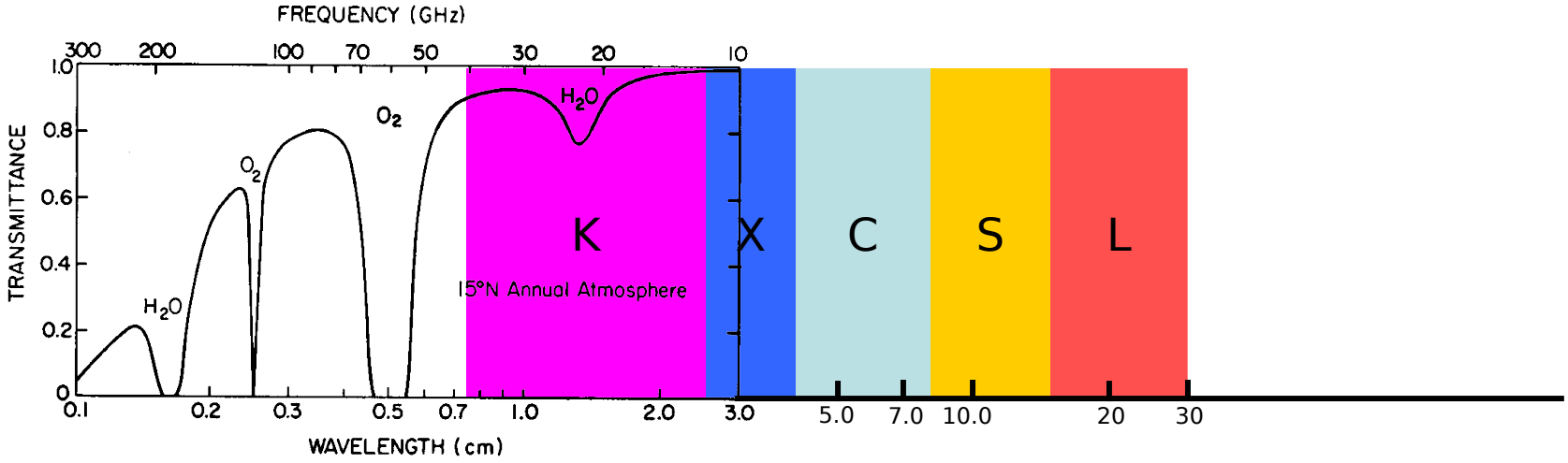

Ahmed, *et al.*, 1990; Raney, 1998

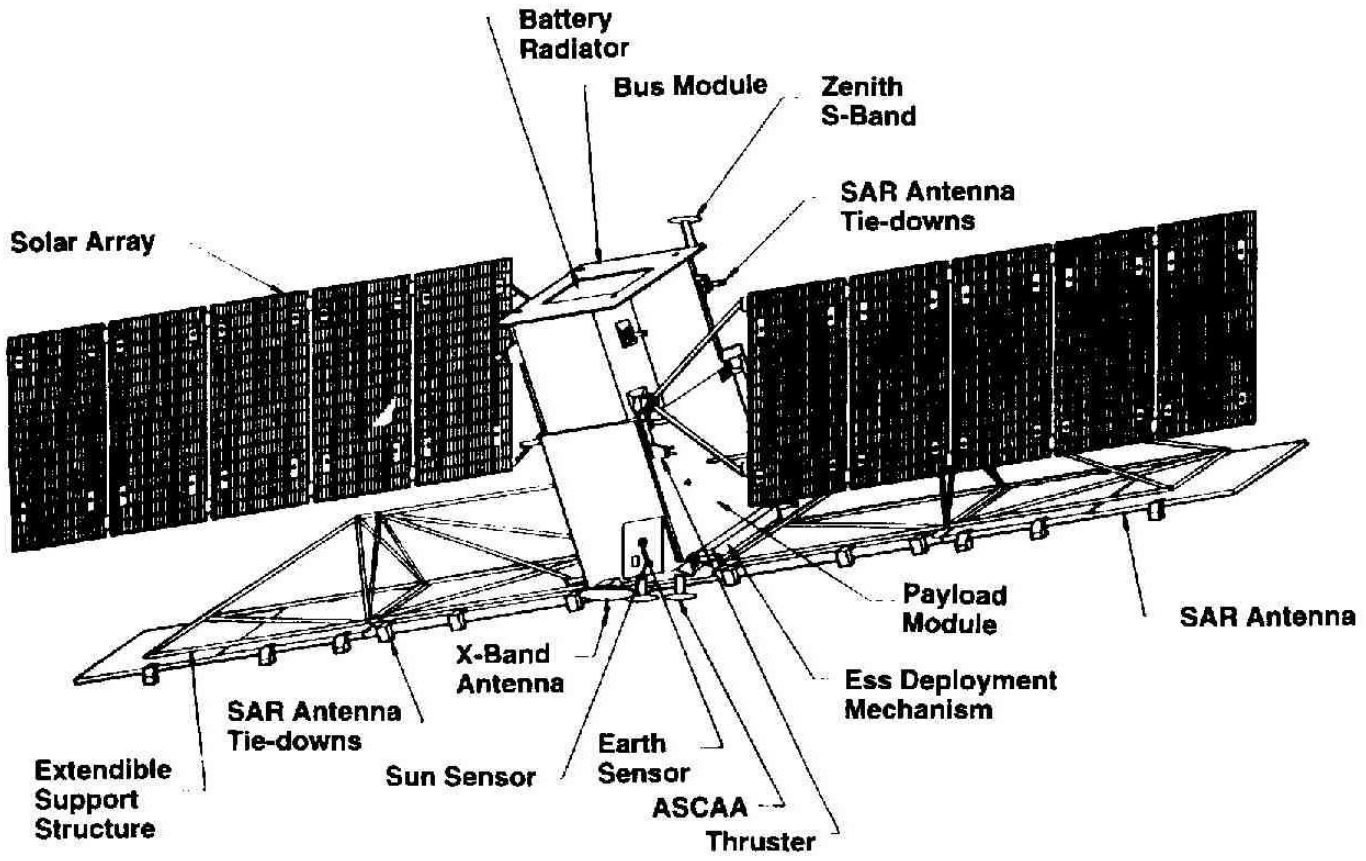

Figure 13.9. The configuration of the RADARSAT spacecraft; the antenna measures 15 m by 1.5 m. (Figure 1 from Moore *et al.* 1993, © 1993 Canadian Aeronautics and Space Institute, used with permission).

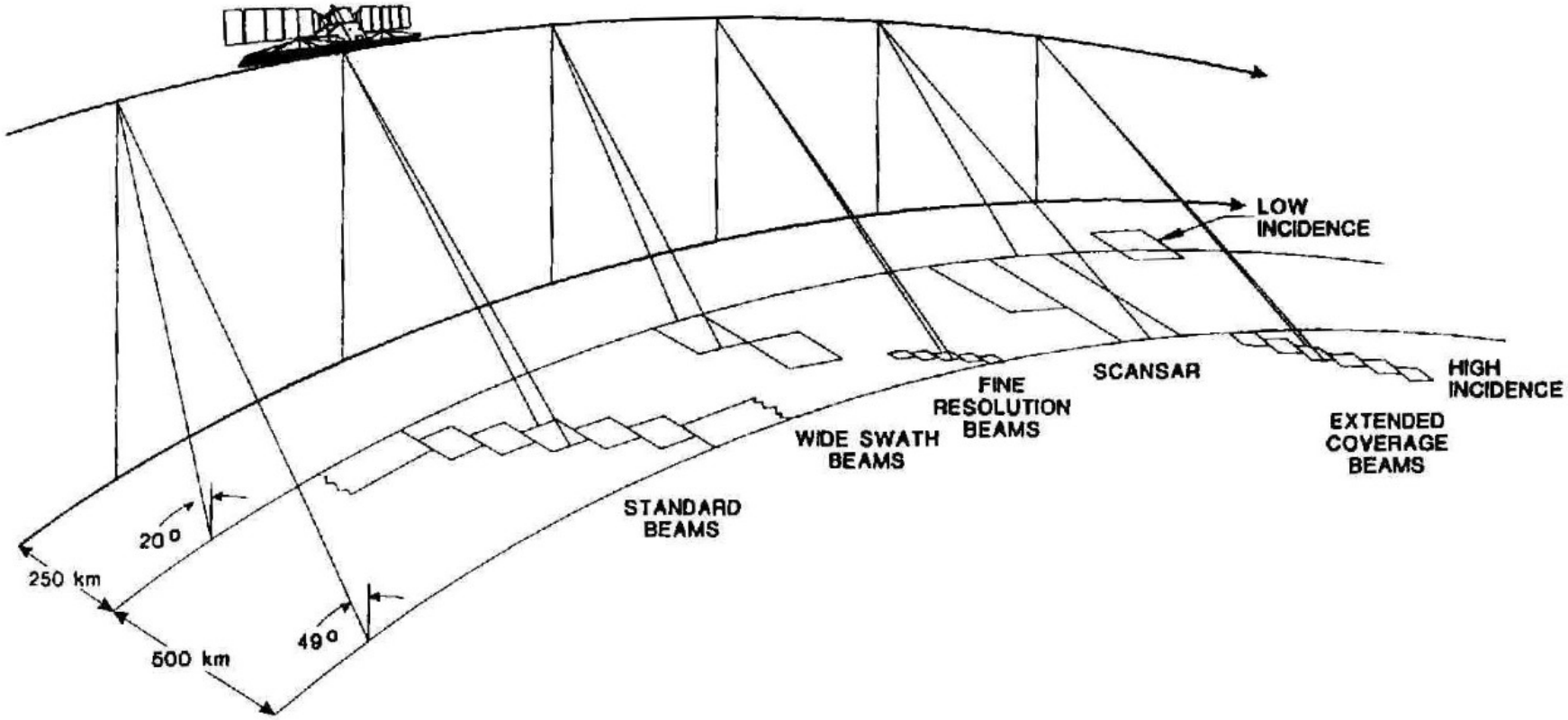

Figure 13.11. The different imaging modes for RADARSAT; see text and Table 13.3 for additional description (Figure 1 from Luscombe *et al.*, 1993, © 1993 Canadian Aeronautics and Space Institute, used with permission).

Large Wave Characteristics

JERS-1/SAR IMAGE OF THE SEA OF JAPAN

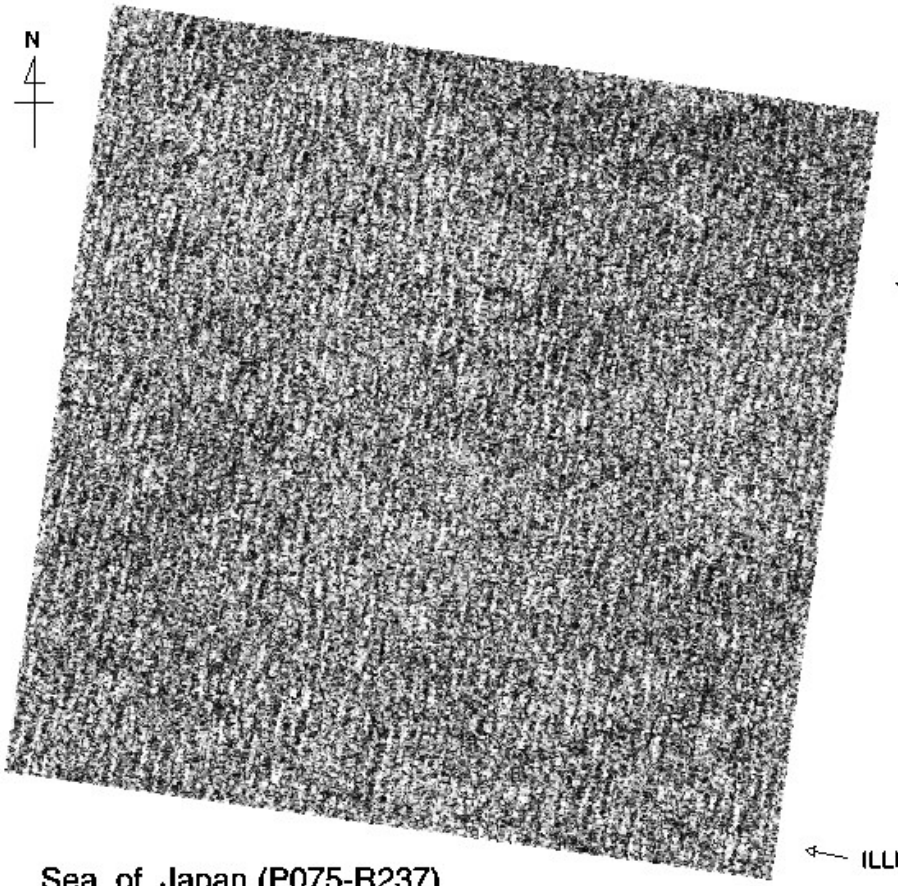

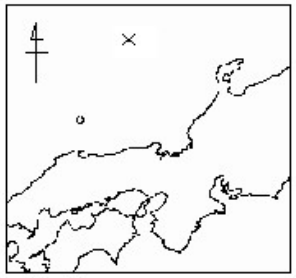

Observation area

This image may show ocean waves. In this area, it was blowing hard from the west for the last 12 hours.

Sea of Japan (P075-R237)
1992.10.25 1:43:05.713 (UT)

NASDA 宇宙開発事業団 RESTEC

JERS-1/SAR OCEAN WAVE SPECTRUM

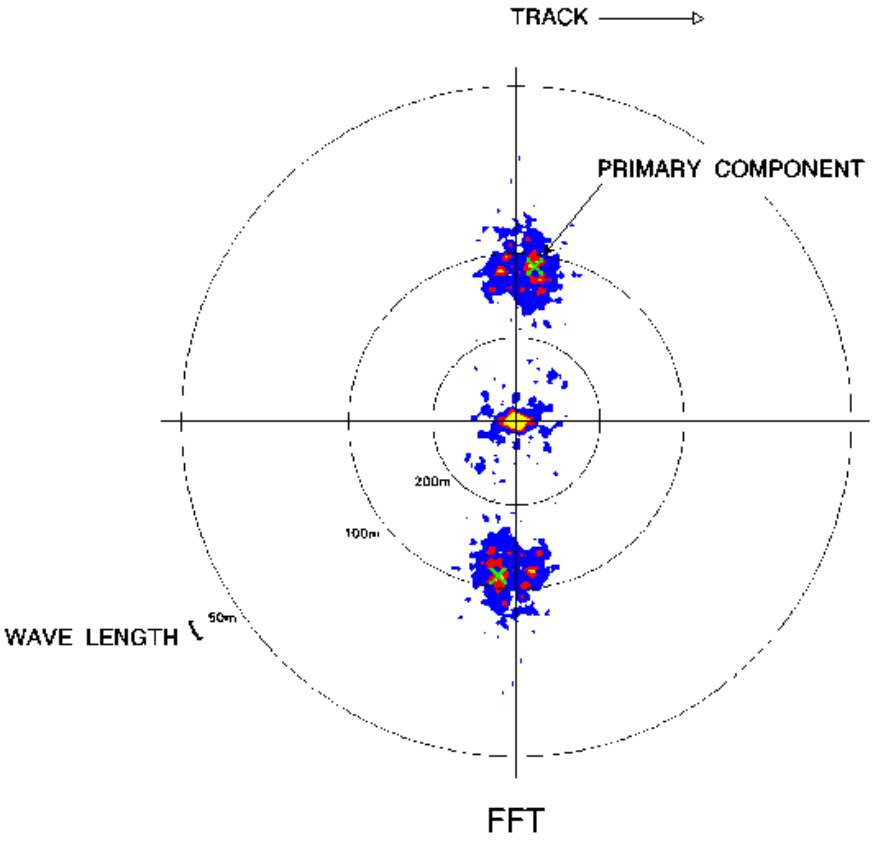

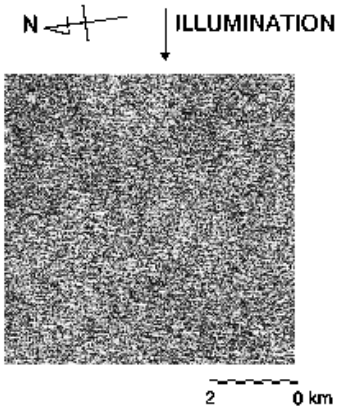

Original
Sea of Japan (P075-R237)
1992.10.25 1:43:05.713 (UT)

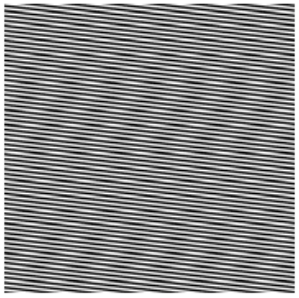

Inv. FFT

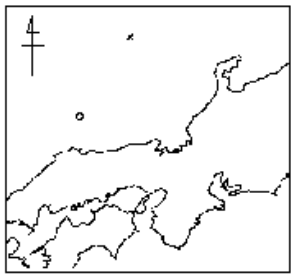

Observation area

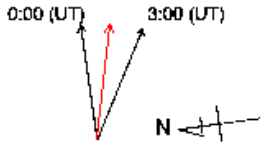

WIND DIRECTION AND
WAVE DIRECTION (RED)

In this area, it was blowing hard from the west for the last 12 hours.
The wave direction calculated from JERS-1/SAR ocean wave spectrum agree with the wind direction.

NASDA 宇宙開発事業団 RESTEC

SeaSat Satellite

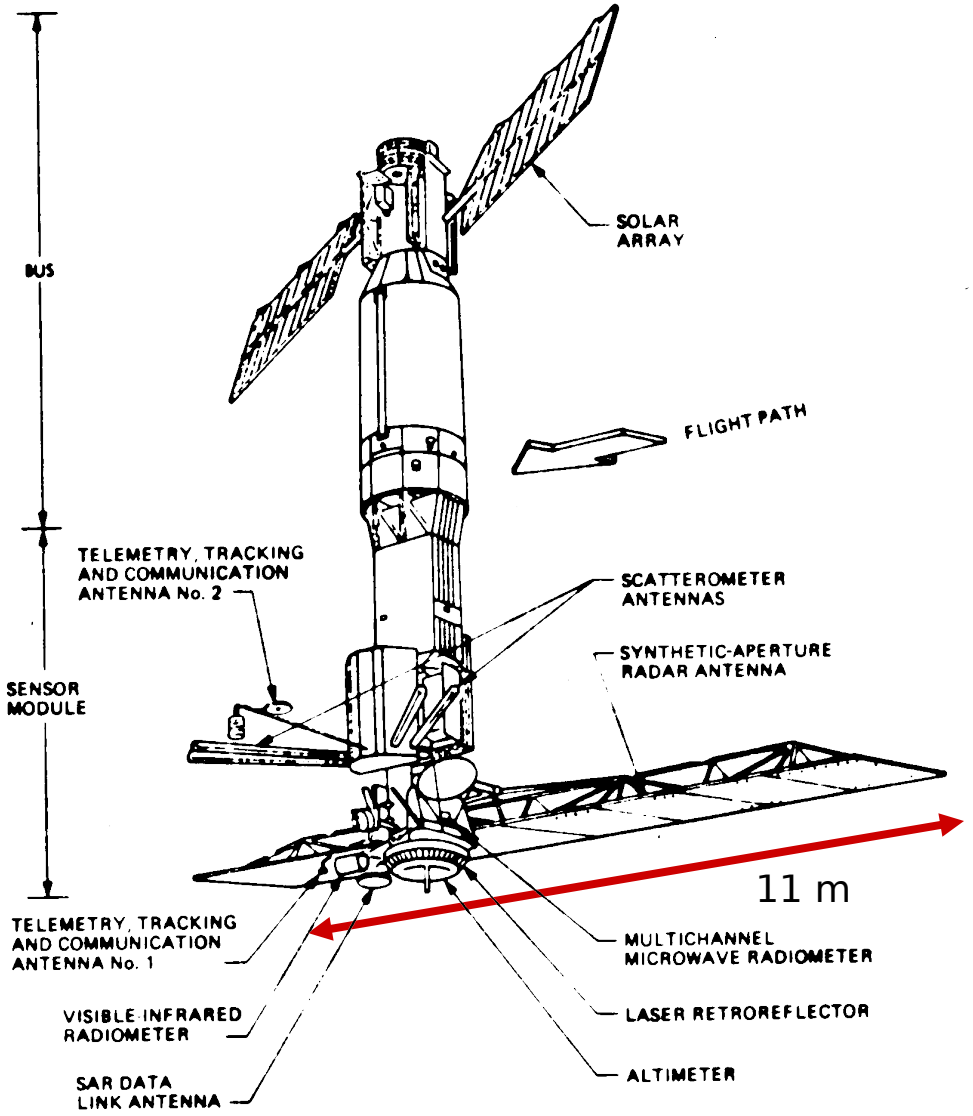

Satellite motion

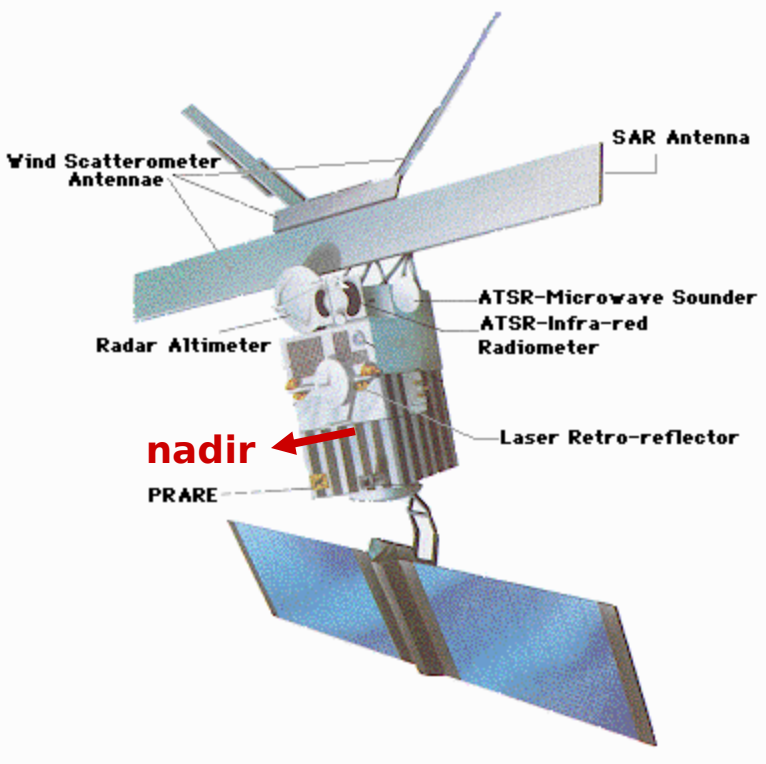

ERS Satellite

Seasat SAR (*Synthetic Aperture Radar)*
L-band, HH polarization, fixed look angle
1275 MHz (23.5 cm) band
100 km swath width at 25 m resolution
Transmitted Pulse Length 33.4 microseconds
Antenna Dimensions 10.74 m x 2.16 m
Antenna Look Angle 20 degrees from vertical
Pulse repetition frequency (PRF) 1463-1640 Hz
Incidence angle on the surface 23 degrees +/- 3 degrees across the swath

RADARSAT	5.3 GHz (C-Band)
ERS	5.3 GHz (C-Band)

The RADARSAT 2
Synthetic Aperture Radar (SAR) will acquire data at **horizontal (HH)**, **vertical (VV)** and **cross (HV)** polarizations over a range of resolutions from 100 to three metres.

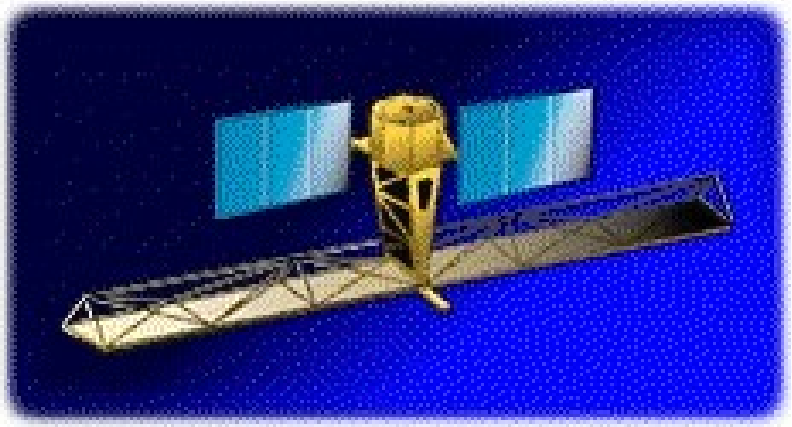

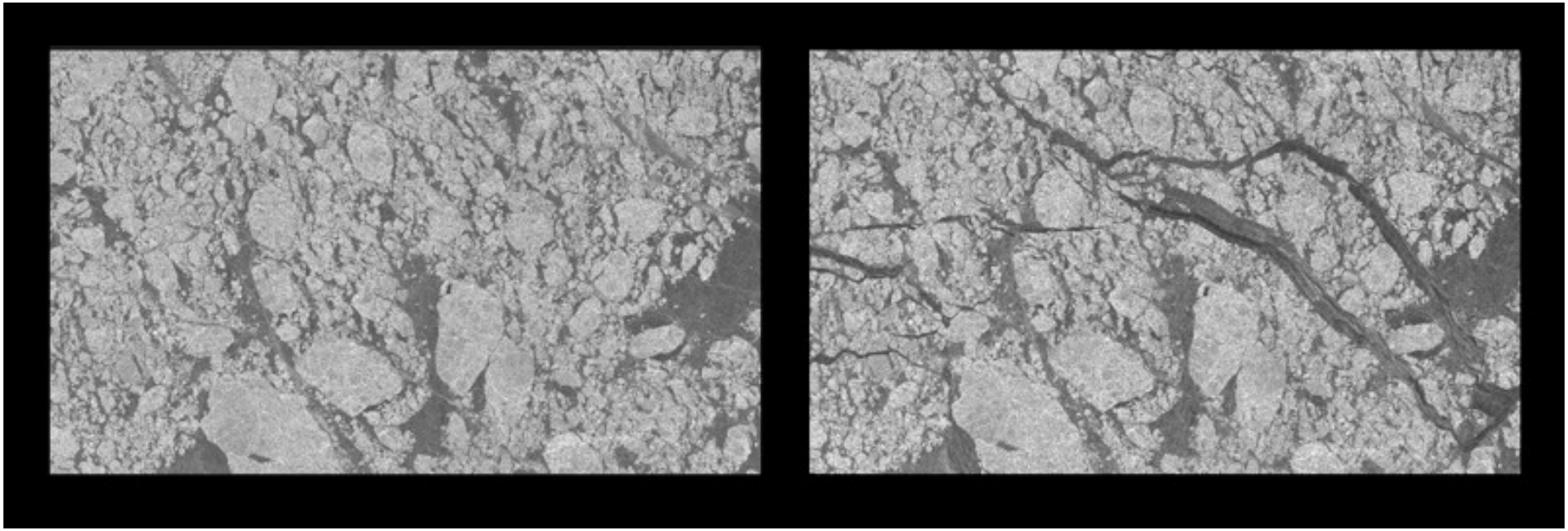

Day 1

Day 9

Radarsat data 96 x128km images

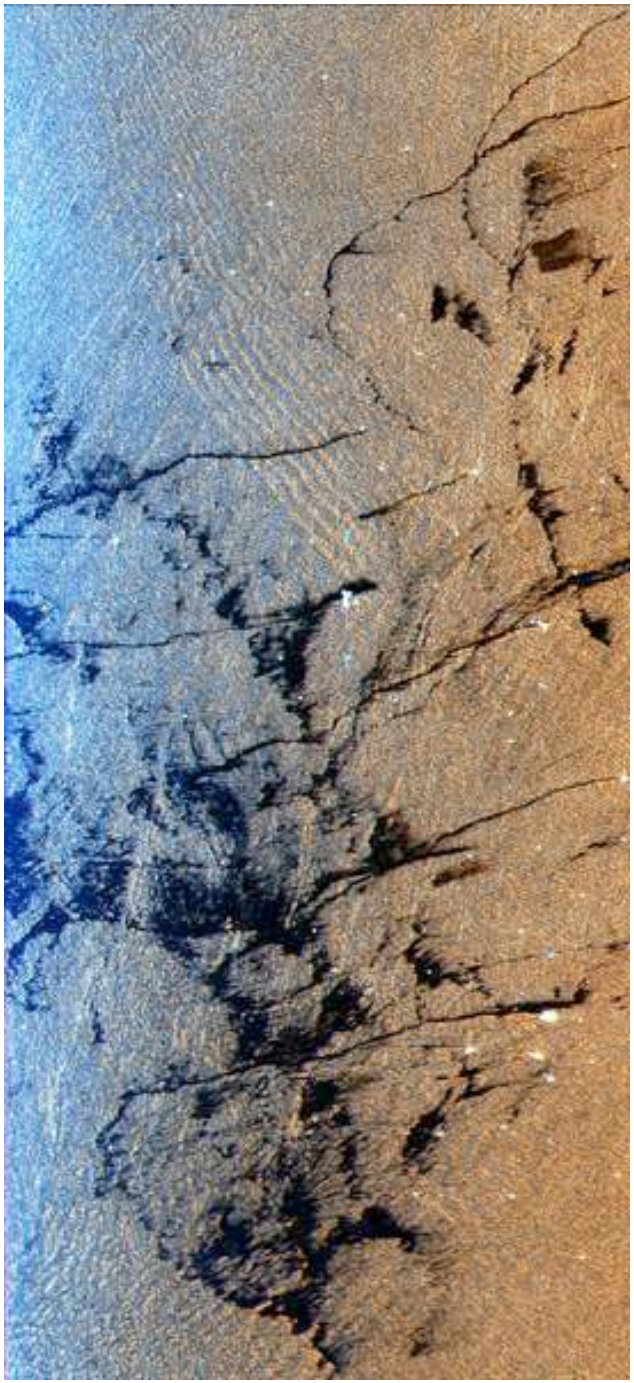

SIR-C/X-SAR (shuttle)

Offshore drilling field - Indian Ocean
20km x 45km Oct. 9, 1994

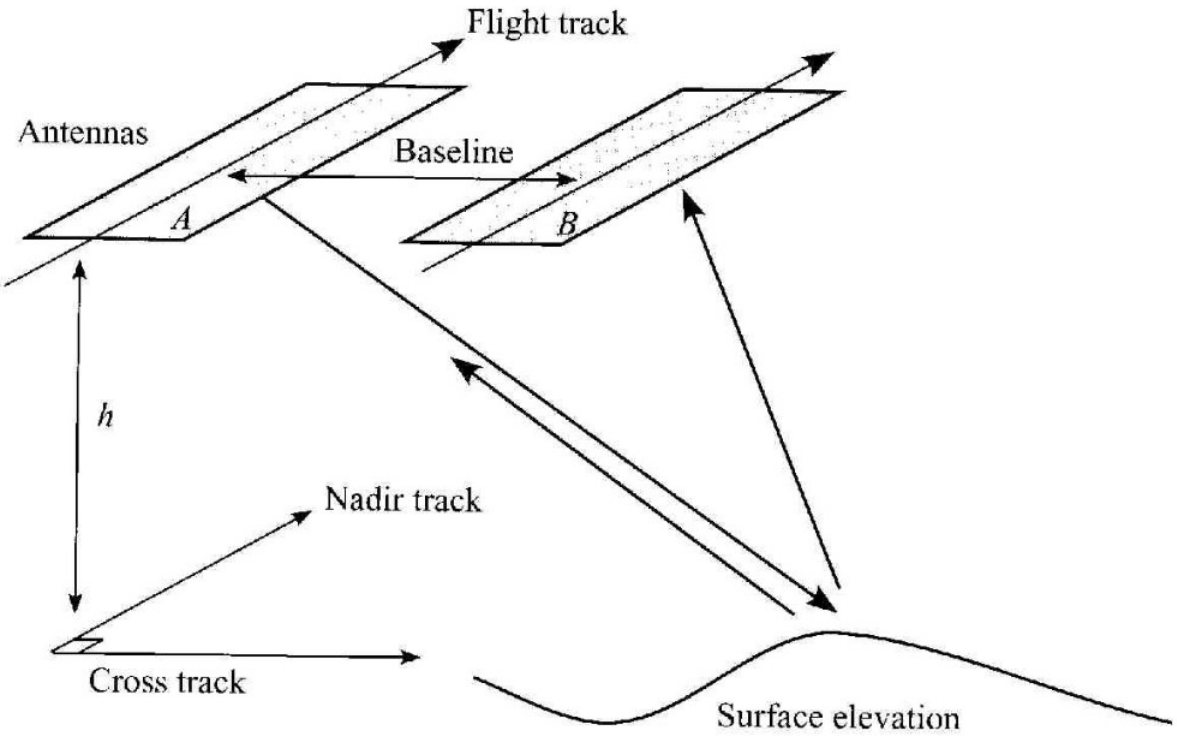

Figure 13.3. The geometry of a cross-track interferometer. The two antennas are at a specific altitude in a parallel track, and are separated by a precisely determined baseline. The antennas make simultaneous observations of the same surface area from two different locations.